LASER & PHOTONICS REVIEWS
www.lpr-journal.org

Ultrafast Laser Printing Green–Red Dual-Phase Perovskite Quantum Dots in Glass

Han Xiao, Ronghua Chen, Zhehong Zhou, Bing Lin, Tao Pang, Jidong Lin, Ruidan Zhang,* Ping Huang, An Xie, and Daqin Chen**

Flexible regulation of local chemistry and band gap of perovskite quantum dots (PeQDs) is crucial for exploring their new functionalities and device applications. In this work, a strategy based on the combination of femtosecond (fs) laser-irradiation and thermal treatment to effectively manipulate chemical composition and emitting wavelength of PeQDs in amorphous glass, is reported. The engineering of ultrafast laser-induced thermal effect enables to induce in situ nucleation/growth of dual-phase PeQDs within an individual glass matrix. By elevating heat-treatment (HT) temperature, I^- ions are driven to surmount the diffusion barrier into the PeQDs lattice, leading to a tunable emission wavelength ranging from 613 to 647 nm. Besides, it is verified that the temperature-dependent diffusion rate of I^- ions plays a pivotal role in affecting luminescent efficiency and color of the dual-phase glass. Finally, fs laser direct writing of multi-color patterns is presented, which provides a flexible method to develop new encryption/decryption technology for information security and anti-counterfeiting.

1. Introduction

Perovskite quantum dots are considered as extremely promising materials for the fabrication of high-performance optoelectronic devices because of their exceptional physical and chemical properties including high photoluminescence quantum efficiency (PLQY, up to 90%), narrow full width at half maximum (FWHM) and tunable emissions.[1–3] As a consequence, PeQDs show broad application prospect in the fields of light-emitting diodes (LEDs),[4–6] photodetectors,[7,8] solar cells,[9,10] lasers[11–14] and so on. The tuning of optical band gap and PL wavelength of PeQDs can be achieved by controlling the sizes and halogens.[15,16] For example, introducing different Cl or I precursors to $CsPbBr_3$ PeQDs facilitates rapid anion exchange, allowing regulation of the emitting color across full spectrum of visible light.[1,17] Although PeQDs have excellent optical properties, low structural stability has been always a major obstacle to the advancement of practical perovskite devices. The inherent ionic crystal feature and substantial surface energy make PeQDs susceptible to degradation when exposed to light, oxygen, water, and elevated temperature,[18–22] inevitably leading to a reduction in luminescent efficiency. Encapsulation of PeQDs is one of the potential strategies for addressing stability issue.[23,24] Despite various suitable materials, such as porous materials,[25] metal–organic frameworks (MOFs),[26] and core/shell,[27] have been utilized to isolate PeQDs from external environment to a certain extent, these materials manifest instability under extreme conditions and require extra processing steps. On this basis, robust inorganic glass has been regarded as an ideal host for PeQDs owing to its high transmittance, good physicochemical stability, low expansion coefficient and easy machining.[28–34] Nevertheless, high structure rigidity of solid glass network makes it difficult to regulate the halogen ions and PL performance of PeQDs within glass.[35]

H. Xiao, R. Chen, Z. Zhou, B. Lin, J. Lin, R. Zhang, D. Chen
College of Physics and Energy
Fujian Normal University
Fuzhou 350117, P. R. China
E-mail: fjnu_lb@fjnu.edu.cn; rdzhang@fjnu.edu.cn; dqchen@fjnu.edu.cn

T. Pang
Huzhou Key Laboratory of Materials for Energy Conversion and Storage
College of Science
Huzhou University
Huzhou 313000, P. R. China

P. Huang
State Key Laboratory of Structural Chemistry
Fujian Institute of Research on the Structure of Matter
Chinese Academy of Sciences
Fuzhou 350002, P. R. China

A. Xie
School of Materials Science and Engineering
Xiamen University of Technology
Xiamen 361024, P. R. China

D. Chen
Fujian Provincial Collaborative Innovation Center for Advanced High-Field Superconducting Materials and Engineering
Fuzhou 350117, P. R. China

D. Chen
Fujian Provincial Engineering Technology Research Center of Solar Energy Conversion and Energy Storage
Fuzhou 350117, P. R. China

The ORCID identification number(s) for the author(s) of this article can be found under https://doi.org/10.1002/lpor.202401258

DOI: 10.1002/lpor.202401258

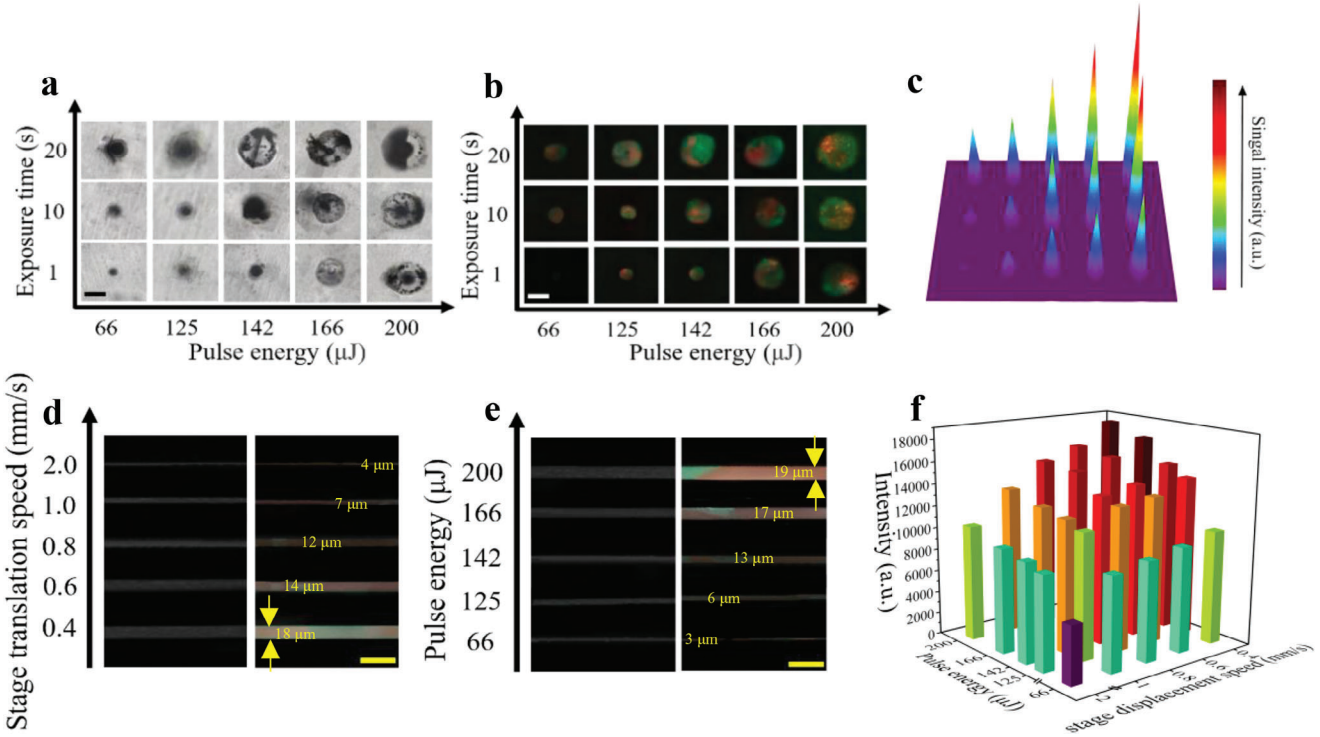

Figure 1. a,b) Microscopic optical images of laser-irradiated dots by using different pulse energies and exposure times taken under natural light and 365 nm UV light. Scale bar: 50 μm. c) Integrated PL intensity mapping with emitting wavelength of 514 and 613 nm recorded from (b). Optical images taken under daylight (left) and 365 nm UV light (right) for laser-written PeQDs lines d) under different displacement speeds and e) under different pulse energies. Scale bar: 50 μm. f) PL intensity mapping corresponding to (d, e).

Recently, fs laser direct writing has been shown to be an effective way to induce crystallization of PeQDs within glass matrix. Ultrafast laser serves as effective localized heat sources for controlling element redistribution and designing chemical compositions, which is crucial for optoelectronic devices such as displays and optical data storage. For example, 3D direct lithography of composition-tunable PeQDs patterns in the Cl^{-}-Br^{-}-I^{-} tri-doped glass and engineering the local chemistry in the B-site Cd/Pb mix-cation system to achieve pure blue emissive PeQDs have been reported previously.[36,37] However, the above method needs continuous adjustment of fs laser irradiation conditions to modulate the proportion of halogen ions and alter the band gap of the perovskite structure, and it is hard to control anion exchange to produce dual-phase PeQDs within an individual glass matrix.

Herein, we report on regulation of I^{-} ionic diffusion to engineer the composition and bandgap in glass through a combination of fs laser irradiation and heat-treatment processes. Simultaneous printing of green&red PeQDs in the Br&I mixed glass is achieved by employing laser-induced nanophase separation and ion exchange. The emitting wavelength is tuned from 613 to 647 nm by elevating HT temperature, which can promote more I^{-} ions to move into liquid perovskite area from glass melt. In addition, we also find that halogen vacancies caused by low diffusion rate of I^{-} ions at low HT treatment temperatures are the primary reason for PL quenching of pure I glass. The green&red emissive PeQDs protected by the glass matrix show excellent optical performance and robustness. Patterning of color-tunable PeQDs holds potential applications in three-dimensional displays, optical data storage, and information security.

2. Results and Discussion

Borosilicate precursor glasses (PGs) containing Cs/Pb/Br/I elements (Table S1, Supporting Information) are designed and prepared. HT serves as a conventional approach for in situ nucleation/growth of PeQDs within the glass matrix. As shown in Figure S1 (Supporting Information), X-ray diffraction (XRD) patterns of these glass samples after HT at 500 °C show only amorphous halo, indicating that the crystallization of $CsPb(Br/I)_3$ PeQDs cannot be achieved in the present glasses via direct thermal treatment. Therefore, a 1030 nm fs laser with a repetition frequency of 10 kHz and a pulse duration of 300 fs is used to induce the growth of PeQDs. The energy absorption of fs laser in the focal region is achieved through nonlinear processes, such as multi-photon ionization,[38] tunnel effect[39] and avalanche ionization.[40] During the nonlinear absorption and energy transfer process, once the energy deposition exceeds a certain threshold, the chemical bonds within the atomic groups of glass network are disrupted, contributing to the atom rearrangement and the formation of crystal nucleus.[41,42] Absorption spectra (Figure S2, Supporting Information) and Raman spectra (Figure S3, Supporting Information) of precursor glass without/with fs laser irradiation are recorded. Evidently, the sample irradiated by fs laser has distinct exciton absorption peaks and several crystalline Ra-

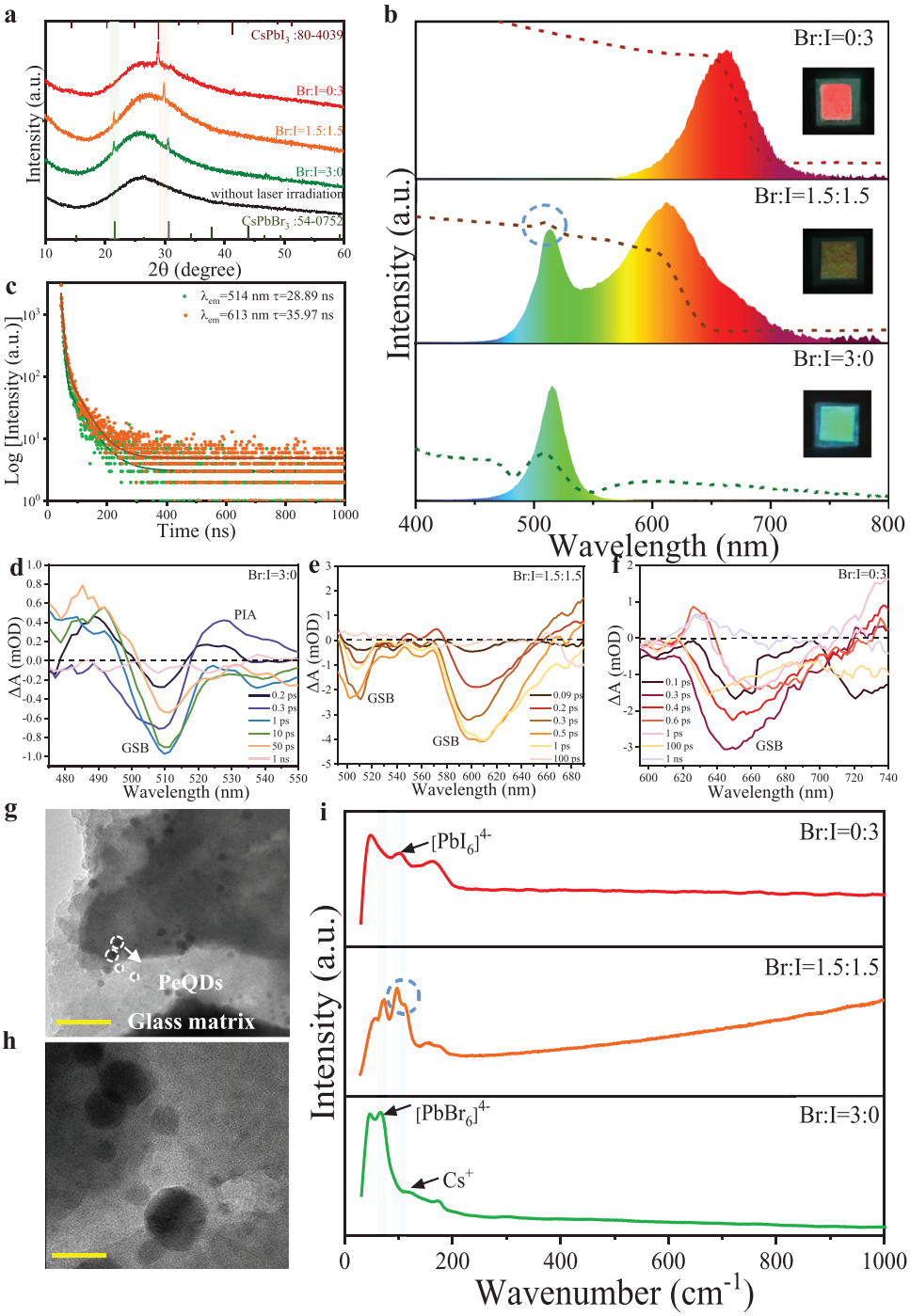

Figure 2. a) XRD patterns, b) absorption and PL spectra, c) PL decay curves by monitoring green emission and red one, d–f) fs-TA spectra, g,h) TEM and HRTEM images of the Br&I glass. Scale bar in (g): 20 nm. Scale bar in (h): 5 nm, i) Raman spectra for the pure Br glass, pure I glass and Br&I glass.

man signals, confirming the feasibility of the laser-induced in situ nucleation/growth of PeQDs.

As shown in **Figure** 1a, taking the Br&I glass with Br/I ratio of 1.5:1.5 as a typical sample, a regularly shaped dot can be observed around the laser focal spot via an optical microscope. With increase of laser pulse energy and extension of exposure duration, the size of the dot progressively enlarges. Under the excitation of 365 nm UV light, apparent green and orange–red colors can be captured, and the luminescence is well confined within laser-irradiated dots (Figure 1b). This confirms the successful growth of green-red dual-phase PeQDs in glass. As shown in Figure 1c, the formation of dual-phase PeQDs in the laser-irradiated region is clearly captured by the integrated PL intensity. It seems that PeQDs in glass is affected by laser pulse energy and exposure time.

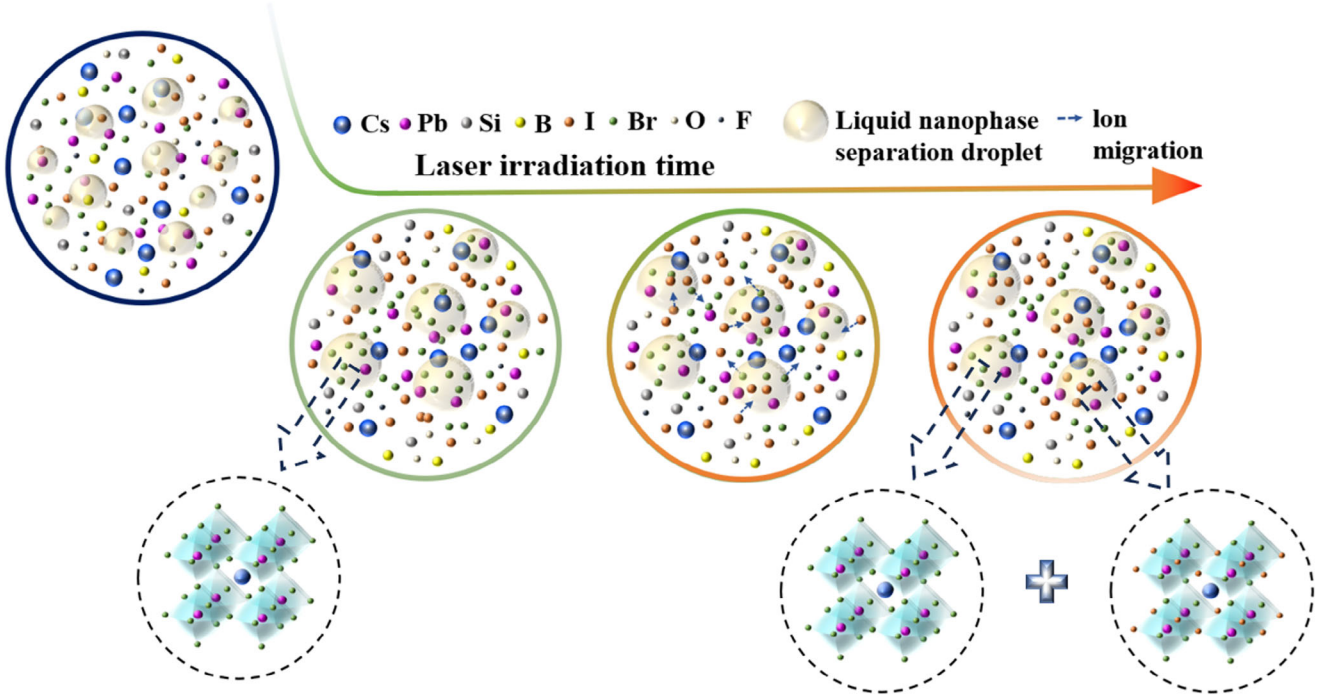

Scheme 1. Schematic of ultrafast laser-induced liquid nanophase separation and I-to-Br ion exchange in the Br&I glass.

When the laser irradiation time is less than 1s, luminescence cannot be detected. Increasing the pulse energy or extending the exposure time can yield more PeQDs and enhance the emission intensity. In addition, the line of PeQDs is written by changing the displacement speed of the sample platform (Figure 1d,e). As the stage movement speed increases, the width of the line becomes narrower and the PL intensity decreases accordingly (Figure 1f). This trend is also observed in laser-induced PeQDs for the pure Br glass and the pure I glass (Figures S4 and S5, Supporting Information). Herein, the optimal laser parameters with a pulse energy of 200 μJ, repetition frequency of 10 kHz, average power of 500 mW and moving speed of 0.4 mm s^{-1} are adopted in the following section (Figure S5, Supporting Information).

The laser-induced dual-phase precipitation in the glass is investigated by XRD patterns and PL spectra (**Figure 2**a,b). The pure Br glass shows diffraction peaks at 21.6° and 30.6° corresponding to the (110) and (200) planes of cubic $CsPbBr_3$ with typical green emission, while the pure I glass exhibits a peak at 28.9° assigned to (200) plane of cubic $CsPbI_3$ with red emission. Impressively, for the Br&I glass, diffraction peak at 21.6° assigned to $CsPbBr_3$ and the one at 29.7° ascribed to $CsPb(Br/I)_3$ are simultaneously detected. This is confirmed by its PL behavior, where both 514 nm green emission and 613 nm red emission are recorded from PL spectrum of the Br&I glass (Figure 2b). In addition, the corresponding decay of the fluorescence signals can be fitted by a tri-exponential function and the lifetimes of the three components are summarized in Table S2 (Supporting Information). The PL decay of $CsPb(Br/I)_3$ (35.97 ns) is observed to be longer than that of $CsPbBr_3$ (28.89 ns) (Figure 2c). It suggests that there is a strong dependence of Kane energy on the halide anion, which may arise from the contribution of mixed s-p orbital in the lowest energy valence band.[43,44] The typical femtosecond transient absorption (fs-TA) spectra of samples excited by 450 nm are shown in Figure 2d-f and Figure S6 (Supporting Information). Within the probed time window, fs-TA spectra are dominated by a ground-state bleach (GSB) and a photon induced absorption (PIA). The former can be attributed to carrier state-filling, and the latter is assigned to bandgap renormalization of carriers.[45,46] It is evident that a distinct GSB signal for the pure Br glass and pure I glass and two GSB signals at 508 nm and 607 nm for the Br&I glass, which aligns well with their exciton absorption behaviors (Figure 2b). The presence of two independent PeQDs in glass is also confirmed by transmission electron microscopy (TEM). Figure 2g clearly presents spherical-like PeQDs dispersed in the glass matrix. High-resolution TEM (HRTEM) images taken in the laser writing region show crystal phases with interplanar distances of 2.65 and 2.12 Å, being consistent with $CsPbBr_3$ (210) and $CsPb(Br/I)_3$ (220) crystal planes (Figure 2h; Figure S7a,b, Supporting Information). The average sizes are evaluated to be 3.77 and 5.80 nm, respectively (Figure S7c,d, Supporting Information). In addition, Raman spectrum for the Br glass manifest peaks at 72 and 122 cm^{-1} representing the vibration of the $[PbBr_6]^{4-}$ octahedron and the motion of Cs^+ in $CsPbBr_3$ (Figure 2i, bottom).[47] The presence of one peak at 96 cm^{-1} for the pure I glass is assigned to symmetric tensile vibration mode of Pb—I bond in $CsPbI_3$ (Figure 2i, top).[48] And the splitting of Raman signals at 94–123 cm^{-1} for the Br&I glass (Figure 2i, middle) evidences the occurrence of halogen exchange between Br and I, resulting in the formation of $CsPb(Br/I)_3$ PeQDs in addition to $CsPbBr_3$ ones in the glass matrix.

The dynamical process of constructing two different PeQDs in the Br&I glass system after fs laser irradiation is proposed (**Scheme 1**). Ultrafast laser can inject energy at a faster time than the lattice thermal diffusion near the focal point at a depth of

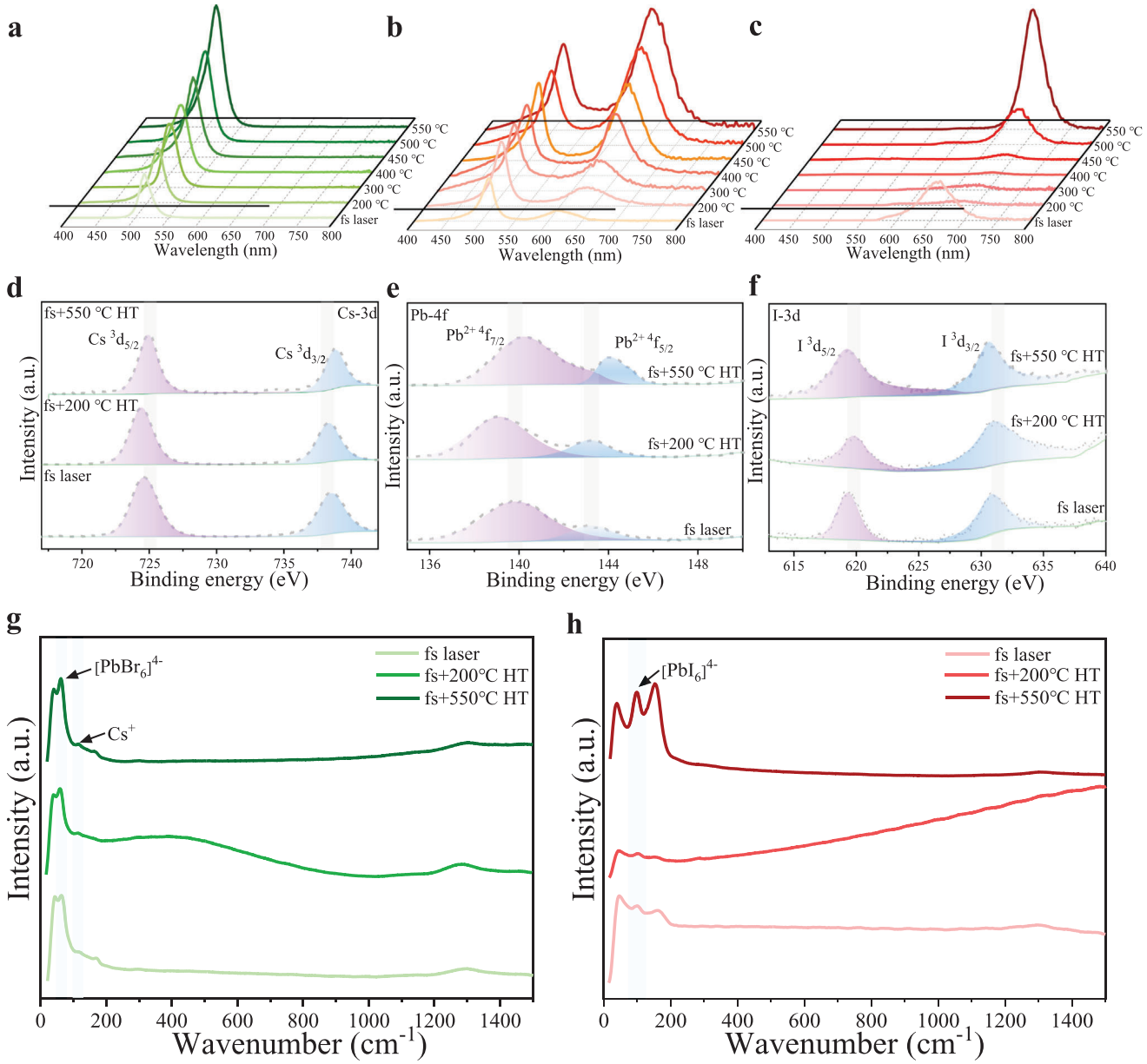

Figure 3. a–c) PL spectra of the laser-irradiated pure Br glass, Br&I glass and pure I glass treated with different HT temperatures. High-resolution XPS spectra of d) Cs, e) Pb, and f) I for the pure I glass, and Raman spectra of g) the pure Br glass and h) the pure I glass via a combination of fs laser irradiation and HT.

0.2 mm from the glass surface, which leads to intense heat accumulation and elevates the local pressure and temperature above the liquidus of the studied glass to facilitate nanophase separation. In comparison to I^-, Br^- has a stronger complexation affinity to Pb^{2+}, lighter ionic weight, smaller radius and faster ion migration rate, allowing for the separation of Br-rich liquid perovskite phase from the glass. Under continuous laser irradiation, the ion exchange of I^- to Br^- driven by the chemical potential gradient occurs, causing I^- ions diffusing from the surrounding liquid glass into Br-dominant liquid perovskite domains. Finally, these liquid perovskite domains become ordered and crystallize into dual-phase $CsPbBr_3$ and $CsPb(Br/I)_3$ PeQDs during cooling.

To further explore the halogen regulation in PeQDs, subsequent HT with various temperatures (200–550 °C) were exerted on the laser-written pure Br glass, Br&I glass and pure I glass (**Figure 3a-c**). For the pure Br glass, besides gradual enhancement of PL, only slight red-shift of 2 nm is observed for PL of $CsPbBr_3$ PeQDs within temperature range of 200–550 °C (Figure 3a). The decay lifetime remains ≈30 ns (Figure S8a, Supporting Information). For the Br&I glass, similar PL enhancement is found for the dual-phase $CsPbBr_3$ and $CsPb(Br/I)_3$ PeQDs, but obvious PL red-shift from 613 nm (200 °C) to 647 nm (550 °C) is evident for the $CsPb(Br/I)_3$ PeQDs (Figure 3b), indicating incorporation of more I^- ions into the $CsPb(Br/I)_3$ lattice with elevation of HT

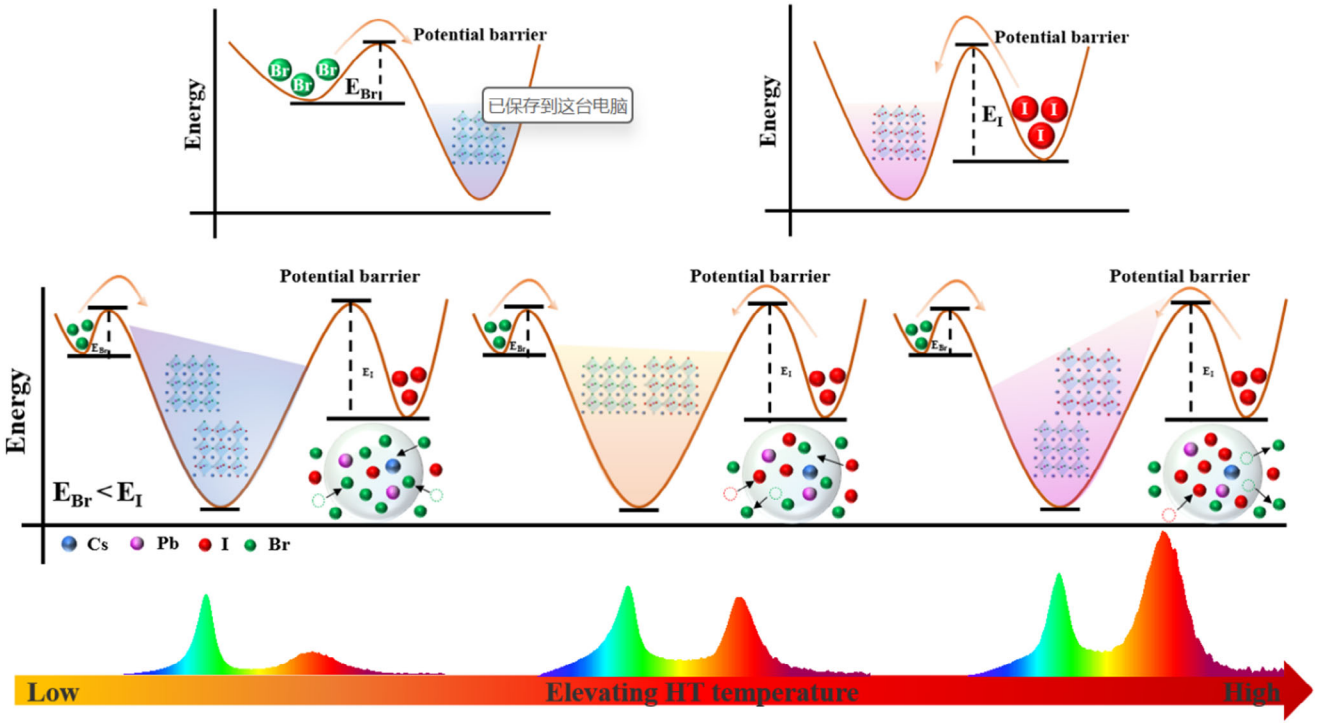

Scheme 2. Schematic of HT temperature-dependent diffusion of Br^- ions and I^- ions from glass matrix to perovskite crystalline phase in the Br&I glass.

temperature. More interestingly, for the pure I glass, PL of $CsPbI_3$ PeQDs will be quenched (Figure 3c) and the corresponding decay lifetime will be significantly elongated from 120 ns to ≈2000 ns (Figure S8b, Supporting Information) after HT at a low temperature (200–450 °C); Further elevating HT temperature up to 550 °C will remarkably shorten decay lifetimes to 153 ns and enhance PL intensity by approximately three times.

Herein, taking the pure I glass as a typical sample, X-ray photoelectron spectroscopy (XPS), temperature-dependent PL spectra and Raman spectra are recorded to analyze microstructure evolution of laser-printing PeQDs in glass via HT. As for the Pb 4f and Cs 3d XPS profiles, the binding energy shift of the sample upon 200 °C low-temperature HT is lower than that of the initial fs laser irradiate one (Figure 3d,e). Following HT at 550 °C, both two peaks shift to a higher binding energy and the I 3d peak shows a reversed change (Figure 3d-f), which is attributed to the stronger binding between Pb and halogen in Pb-I octahedron of PeQDs. For laser-written $CsPbI_3$ PeQDs, the I/Pb ratio of the sample treated at 200 °C HT decreases clearly from 3.01 to 2.97 (Table S3, Supporting Information), indicating the existence of halogen vacancies (i.e., defect states) on the surface and leading to obvious elongation of PL decay lifetime. However, the ratio of I/Pb increases to 3.07 via high-temperature HT at 550 °C, suggesting that the surface of $CsPbI_3$ PeQDs has anion-rich composition and substantial surface defects are passivated, thereby promoting PL intensity of $CsPbI_3$ PeQDs and significantly shortening PL decay lifetime. Based on temperature-dependent PL spectra for the pure Br samples (Figure S9, Supporting Information), it is evaluated that the exciton binding energy of $CsPbBr_3$ PeQDs gradually enhances with elevation of HT temperature. On the contrary, the exciton binding energy of the pure I glass decreases upon low-temperature HT (Figure S10, Supporting Information), impeding the radiative recombination of excitons. The presence of numerous defects as non-radiative recombination centers inhibits the luminescence of the sample. After high-temperature HT, the sample demonstrates an increased exciton binding energy (Figure S10, Supporting Information), which is reflected in a reduced defect density and an improvement in the efficiency of radiative recombination. Taking into account the data given by Raman tests (Figure 3g,h), it is evident that the diffusion of I^- ions in glass matrix is limited and insufficient to supply the necessary halogen elements for the growth of $CsPbI_3$ at a relatively low HT temperature in comparison to that of $CsPbBr_3$, leading to the weakened Pb-I symmetric tensile vibration signal. The crystal quality of PeQDs will be significantly improved by elevating HT temperature because of the promotion of I^- diffusions and the repairment of surface defects.

Here, we proposed a possible mechanism to illustrate HT temperature-dependent growth of dual-phase PeQDs in glass (**Scheme 2**). Due to its lower diffusion barrier compared to I^- ions, Br^- ions can diffuse from the glass matrix to the lattice at a lower HT temperature, resulting in the preferential formation of Br-rich perovskite phase. For the pure I glass, the high potential barrier for I diffusion will lead to the occurrence of defect states. In this scenario, the main route between photo-excited electrons and trap states is non-irradiation recombination, which is the essential reason for the PL quenching of $CsPbI_3$ PeQDs. Elevating HT temperature facilitates the migration of I^- across the potential barrier within the glass matrix, and the defect states will be reduced or even eliminated, which is conducive to exciton recombination and enhance PL. Therefore, it is understandable that for the Br&I glass, the quality of $CsPbBr_3$ PeQDs is better than that

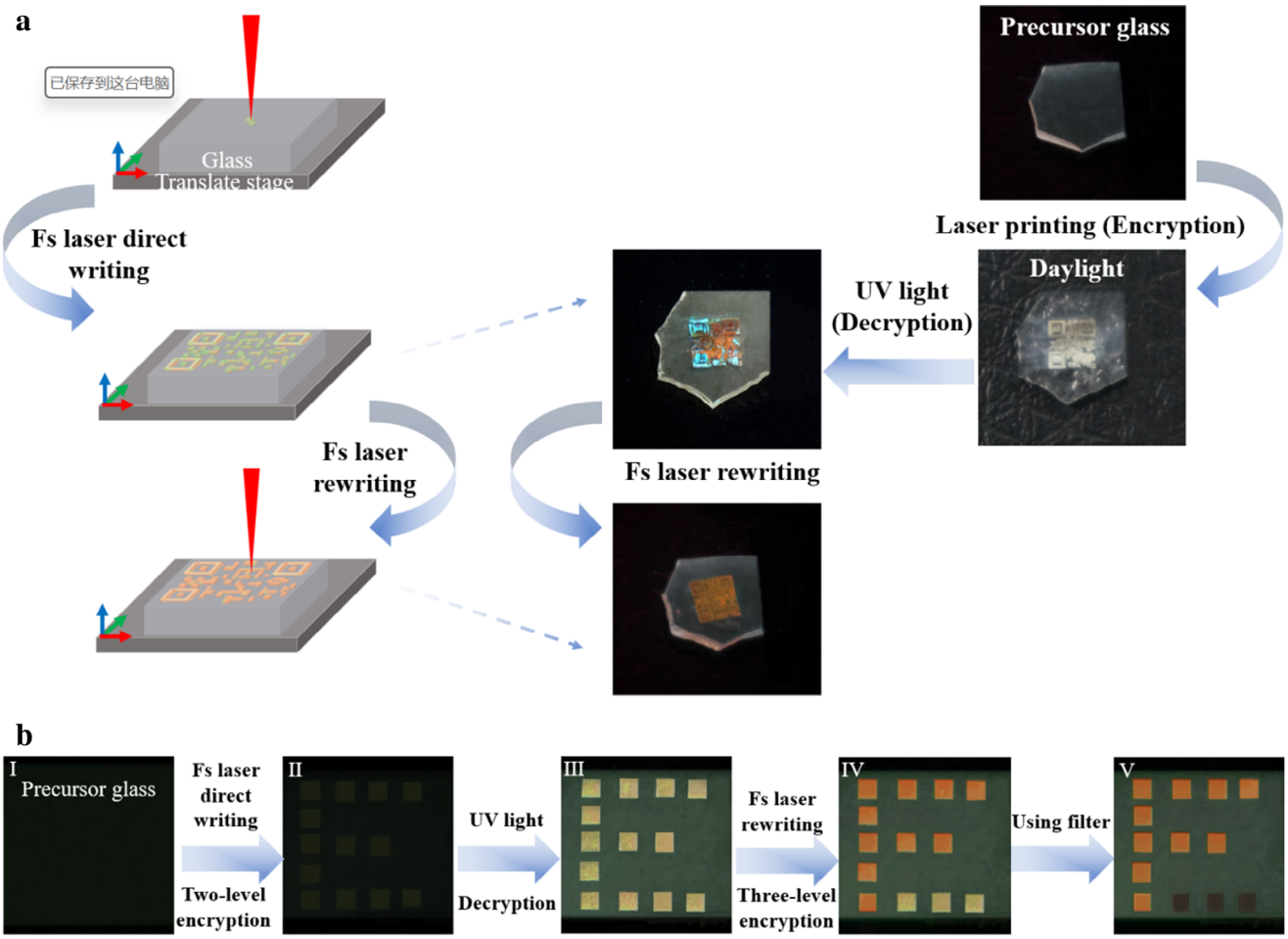

Figure 4. a) Schematic of fs laser-printed Br&I glass based QR code for multi-dimensional data storage. b) Demonstration of fs laser-printed Br&I glass based patterns for the information three-level encryption.

of $CsPb(Br/I)_3$ ones after HT at low temperature, which results in higher green PL intensity than red one (Figure 3b and Scheme 2). Elevating HT temperature not only improves the diffusion rate of Br^- ions to increase the size of the perovskite phases but also promotes the diffusion of I^- ions and improve the quality of mixed halide $CsPb(Br/I)_3$ PeQDs, which be beneficial for the enhanced red emission relative to green one (Figure 3b and Scheme 2).

The heat accumulation effect induced by fs laser enables localized nanophase separation and ion exchange in glass, regulating the chemical composition and PL of PeQDs. Based on the flexibility of laser processing, quick response code (QR code) can be designed for multi-dimensional data storage. The fs laser-printed Br&I glass based QR code show no significant differences in daylight, but displayed distinct colors when exposed to UV light irradiation. The original code exhibits green–red dual colors under UV light irradiation and changes into red one after fs laser rewriting (**Figure** 4a). As depicted in Figure S11 (Supporting Information), the PL of $CsPb(Br/I)_3$ PeQDs exhibits a shift from the initial 613 to 655 nm after the second laser irradiation, accompanied by a significant enhancement in red emission. This color modification is ascribed to the augmented diffusion of I^- ions induced by laser rewriting, resulting in the formation of a substantial quantity of $CsPb(Br/I)_3$ PeQDs via ion exchange. Notably, the PeQDs embedded in glass matrix have superior PL stability (Figure S12, Supporting Information) compared to those synthesized by alternative solution methods.[49,50] This characteristic renders them highly suitable for secure encryption and decryption of key information. Furthermore, three-level encryption of the password can be realized by using the corresponding wavelength filter. The letter "E" pattern is directly printed onto the glass using an ultrafast laser (Figure 4b-II), which can only be decoded when illuminated by a UV lamp (Figure 4b-III). Subsequently, certain specific segments of the code can be modified by repeatedly writing with the same power laser (Figure 4b-IV), employing UV illumination with a 645 nm filter to achieve the letter "F" pattern (Figure 4b-V; Figure S11, Supporting Information).

3. Conclusion

In summary, we demonstrate that the diffusion of I^- ions into PeQDs can be tailored by employing fs laser irradiation combined with heat-treatment. Ultrafast laser-induced phase separation and ion exchange is successfully achieved to generate dual-phase $CsPbBr_3$ and $CsPb(Br/I)_3$ PeQDs in the Br&I glass. The

emission wavelength of $CsPb(Br/I)_3$ PeQDs can be re-modulated by appropriately extending the temperature of thermal treatment and promoting the diffusion of more I^- ions from glass matrix into PeQDs. Furthermore, we have also observed that the ability of I^- ionic diffusion in glass influenced by HT temperature has a discernible impact on the optical properties of PeQDs. Importantly, the PL tunability of PeQDs embedded in glass show superior optical performance and robustness, which has been demonstrated to be applicable for the information encryption/decryption.

Supporting Information

Supporting Information is available from the Wiley Online Library or from the author.

Acknowledgements

This research was supported by National Natural Science Foundation of China (52272141, 51972060, 12074068, 52102159 and 22103012), and Natural Science Foundation of Fujian Province (2020J02017, 2021J06021, 2021J01190 and 2020J01931).

Conflict of Interest

The authors declare no conflict of interest.

Data Availability Statement

The data that support the findings of this study are available from the corresponding author upon reasonable request.

Keywords

$CsPbX_3$, femtosecond laser, glass, luminescent materials, perovskite quantum dots

Received: August 7, 2024
Revised: September 10, 2024
Published online:

[1] L. Protesescu, S. Yakunin, M. I. Bodnarchuk, F. Krieg, R. Caputo, C. H. Hendon, R. Yang, A. Walsh, M. V. Kovalenko, *Nano Lett.* **2015**, *15*, 3692.
[2] J. Song, J. Li, X. Li, L. Xu, Y. Dong, H. Zeng, *Adv. Mater.* **2015**, *27*, 7162.
[3] Y. Su, X. Chen, W. Ji, Q. Zeng, Z. Ren, Z. Su, L. Liu, *ACS Appl. Mater. Interfaces* **2017**, *9*, 33020.
[4] Z. Li, Z. Chen, Y. Yang, Q. Xue, H. L. Yip, Y. Cao, *Nat. Commun.* **2019**, *10*, 1027.
[5] K. Lin, J. Xing, L. Quan, F. P. G. De Arquer, X. Gong, J. Lu, L. Xie, W. Zhao, D. Zhang, C. Yan, W. Li, X. Liu, Y. Lu, J. Kirman, E. H. Sargent, Q. Xiong, Z. Wei, *Nature* **2018**, *562*, 245.
[6] L. Zhao, Y. W. Yeh, N. L. Tran, F. Wu, Z. Xiao, R. A. Kerner, Y. H. L. Lin, G. D. Scholes, N. Yao, B. P. Rand, *ACS Nano* **2017**, *11*, 3957.
[7] Q. Chen, J. Wu, X. Ou, B. Huang, J. Almutlaq, A. A. Zhumekenov, X. Guan, S. Han, L. Liang, Z. Yi, J. Li, X. Xie, Y. Wang, Y. Li, D. Fan, D. B. L. Teh, A. H. All, O. F. Mohammed, O. M. Bakr, T. Wu, M. Bettinelli, H. Yang, W. Huang, X. Liu, *Nature* **2018**, *561*, 88.
[8] H. Gao, J. Feng, Y. Pi, Z. Zhou, B. Zhang, Y. Wu, X. Wang, X. Jiang, L. Jiang, *Adv. Funct. Mater.* **2018**, *28*, 1804349.
[9] N. J. Jeon, H. Na, E. H. Jung, T. Y. Yang, Y. G. Lee, G. Kim, H. W. Shin, S. I. Seok, J. Lee, J. Seo, *Nat. Energy* **2018**, *3*, 682.
[10] E. H. Jung, N. J. Jeon, E. Y. Park, C. S. Moon, T. J. Shin, T. Y. Yang, J. H. Noh, J. Seo, *Nature* **2019**, *567*, 511.
[11] F. Fan, O. Voznyy, R. P. Sabatini, K. T. Bicanic, M. M. Adachi, J. R. Mcbride, K. R. Reid, Y. S. Park, X. Li, A. Jain, R. Quintero-Bermudez, M. Saravanapavanantham, M. Liu, M. Korkusinski, P. Hawrylak, V. I. Klimov, S. J. Rosenthal, S. Hoogland, E. H. Sargent, *Nature* **2017**, *544*, 75.
[12] J. Feng, X. Yan, Y. Zhang, X. Wang, Y. Wu, B. Su, H. Fu, L. Jiang, *Adv. Mater.* **2016**, *28*, 3732.
[13] Y. Jia, R. A. Kerner, A. J. Grede, B. P. Rand, N. C. Giebink, *Nat. Photonics* **2017**, *11*, 784.
[14] B. Tang, H. Dong, L. Sun, W. Zheng, Q. Wang, F. Sun, X. Jiang, A. L. Pan, L. Zhang, *ACS Nano* **2017**, *11*, 10681.
[15] E. Erol, O. Kibrisli, M. Ersundu, A. E. Ersundu, *Chem. Eng. J.* **2020**, *401*, 126053.
[16] C. H. Lu, G. V. Biesold, Y. Liu, Z. Kang, Z. Lin, *Chem. Soc. Rev.* **2020**, *49*, 4953.
[17] Z. Gong, W. Zheng, Y. Gao, P. Huang, D. Tu, R. Li, J. Wei, W. Zhang, Y. Zhang, X. Chen, *Angew. Chem., Int. Ed.* **2019**, *58*, 6943.
[18] W. Lv, L. Li, M. Xu, J. Hong, X. Tang, L. Xu, Y. Wu, R. Zhu, R. Chen, W. Huang, *Adv. Mater.* **2019**, *31*, 1900682.
[19] S. Zou, Y. Liu, J. Li, C. Liu, R. Feng, F. Jiang, Y. Li, J. Song, H. Zeng, M. Hong, X. Chen, *J. Am. Chem. Soc.* **2017**, *139*, 11443.
[20] W. Mao, C. R. Hall, S. Bernardi, Y. B. Cheng, A. Widmer-Cooper, T. A. Smith, U. Bach, *Nat. Mater.* **2021**, *20*, 55.
[21] A. D. Wright, J. B. Patel, M. B. Johnston, L. M. Herz, *Adv. Mater.* **2023**, *35*, 2210834.
[22] H. Zhang, X. Fu, Y. Tang, H. Wang, C. Zhang, W. Yu, X. Wang, Y. Zhang, M. Xiao, *Nat. Commun.* **2019**, *10*, 1088.
[23] Z. Li, E. Hofman, J. Li, A. H. Davis, C. H. Tung, L. Wu, W. Zheng, *Adv. Funct. Mater.* **2018**, *28*, 1704288.
[24] B. Tang, X. Zhao, L. Ruan, C. Qin, A. Shu, Y. Ma, *Nanoscale* **2021**, *13*, 10600.
[25] H. C. Wang, S. Y. Lin, A. C. Tang, B. P. Singh, H. C. Tong, C. Y. Chen, Y. C. Lee, T. L. Tsai, R. S. Liu, *Angew. Chem., Int. Ed.* **2016**, *55*, 7924.
[26] Z. Chen, Z. Gu, W. Fu, F. Wang, J. Zhang, *ACS Appl. Mater. Interfaces* **2016**, *8*, 28737.
[27] V. K. Ravi, S. Saikia, S. Yadav, V. V. Nawale, A. Nag, *ACS Energy Lett.* **2020**, *5*, 1794.
[28] S. Chen, J. Lin, J. Huang, T. Pang, Q. Ye, Y. Zheng, X. Li, Y. Yu, B. Zhuang, D. Chen, *Adv. Funct. Mater.* **2023**, *34*, 2309293.
[29] S. Chen, J. Lin, S. Zheng, Y. Zheng, D. Chen, *Adv. Funct. Mater.* **2023**, *33*, 2213442.
[30] S. Liao, Z. Yang, J. Lin, S. Wang, J. Zhu, S. Chen, F. Huang, Y. Zheng, D. Chen, *Adv. Funct. Mater.* **2023**, *33*, 2210558.
[31] J. Lin, S. Chen, W. Ye, Y. Zeng, H. Xiao, T. Pang, Y. Zheng, B. Zhuang, F. Huang, D. Chen, *Adv. Funct. Mater.* **2024**, *34*, 2314795.
[32] J. Lin, Y. Lu, X. Li, F. Huang, C. Yang, M. Liu, N. Jiang, D. Chen, *ACS Energy Lett.* **2021**, *6*, 519.
[33] I. Konidakis, K. Brintakis, A. Kostopoulou, I. Demeridou, P. Kavatzikidou, E. Stratakis, *Nanoscale* **2020**, *12*, 13697.
[34] I. Konidakis, A. Karagiannaki, E. Stratakis, *Nanoscale* **2022**, *14*, 2966.
[35] J. Li, D. Zhou, Y. Liu, Y. Chen, J. Chen, Y. Yang, Y. Gao, J. Qiu, *ACS Appl. Mater. Interfaces* **2023**, *15*, 22219.
[36] K. Sun, X. Li, D. Tan, H. Jiang, K. Xiong, J. Zhang, B. Xu, Z. Xiao, Z. Li, J. Qiu, *Laser Photonics Rev.* **2023**, *17*, 2200902.
[37] K. Sun, D. Tan, X. Fang, X. Xia, D. Lin, J. Song, Y. Lin, Z. Liu, M. Gu, Y. Yue, J. Qiu, *Science* **2022**, *375*, 307.
[38] G. Mainfray, G. Manus, *Rep. Prog. Phys.* **1991**, *54*, 1333.
[39] A. P. Joglekar, H. H. Liu, E. Meyhöfer, G. Mourou, A. J. Hunt, *Proc. Natl. Acad. Sci. USA* **2004**, *101*, 5856.

[40] J. Noack, A. Vogel, *IEEE J. Quantum Elect.* **1999**, *35*, 1156.
[41] X. Huang, Q. Guo, S. Kang, T. Ouyang, Q. Chen, X. Liu, Z. Xia, Z. Yang, Q. Zhang, J. Qiu, G. Dong, *ACS Nano* **2020**, *14*, 3150.
[42] X. Huang, Q. Guo, D. Yang, X. Xiao, X. Liu, Z. Xia, F. Fan, J. Qiu, G. Dong, *Nat. Photonics* **2020**, *14*, 82.
[43] H. Chung, S. I. Jung, H. J. Kim, W. Cha, E. Sim, D. Kim, W. K. Koh, J. Kim, *Angew. Chem., Int. Ed.* **2017**, *56*, 4160.
[44] N. S. Makarov, S. Guo, O. Isaienko, W. Liu, I. Robel, V. I. Klimov, *Nano Lett.* **2016**, *16*, 2349.
[45] J. S. Manser, P. V. Kamat, *Nat. Photonics* **2014**, *8*, 737.
[46] Y. Yang, D. P. Ostrowski, R. M. France, K. Zhu, J. Van De Lagemaat, J. M. Luther, M. C. Beard, *Nat. Photonics* **2016**, *10*, 53.
[47] J. H. Cha, J. H. Han, W. Yin, C. Park, Y. Park, T. K. Ahn, J. H. Cho, D. Y. Jung, *J. Phys. Chem. Lett.* **2017**, *8*, 565.
[48] K. Sun, D. Tan, J. Song, W. Xiang, B. Xu, J. Qiu, *Adv. Opt. Mater.* **2021**, *9*, 2100094.
[49] H. Hu, L. Wu, Y. Tan, Q. Zhong, M. Chen, Y. Qiu, D. Yang, B. Sun, Q. Zhang, Y. Yin, *J. Am. Chem. Soc.* **2018**, *140*, 406.
[50] W. Wang, J. Li, P. Ni, B. Liu, Q. Chen, Y. Lu, H. Wu, B. Cao, Z. Liu, *ES Mater. Manuf.* **2019**, *4*, 66.